RSC Advances

PAPER

View Article Online
View Journal | View Issue

Cite this: *RSC Adv.*, 2016, **6**, 19417

Preparation of polyetheretherketone composites with nanohydroxyapatite rods and carbon nanofibers having high strength, good biocompatibility and excellent thermal stability

Kai Wang Chan,[a] Cheng Zhu Liao,[b] Hoi Man Wong,[c] Kelvin Wai Kwok Yeung[c] and Sie Chin Tjong*[a]

In recent years, research in the development of polymeric materials for orthopedic implants has become ever more important because the global demand of biocompatible implants has been steadily increasing. Bioinert polyetheretherketone (PEEK) is typically reinforced with bioactive hydroxyapatite microparticles. However, the tensile strength of conventional PEEK/hydroxyapatite microcomposites falls sharply with increasing filler loading. To address low strength and high filler loading issues, nanohydroxyapatite rods (nHA) and carbon nanofibers (CNF) were employed to reinforce PEEK. In this study, molded-grade PEEK pellets, nHA and CNF fillers were melt-mixed and injection molded to form PEEK/nHA and hybrid PEEK/nHA–CNF nanocomposites. The tensile and thermal properties, as well as the bioactivity and biocompatibility of such nanocomposites, were investigated. Tensile test results showed that elastic modulus of PEEK/nHA nanocomposites increases with increasing nHA content. The PEEK/9.3 vol% nHA nanocomposite exhibited higher tensile strength than that of a conventional HAPEX microcomposite. Thermogravimetric measurements indicated that the nHA addition improves the thermal stability of PEEK. Thus, the PEEK/9.3 vol% nHA nanocomposite that had good mechanical, thermal and biological performances was an attractive biomaterial for use in maxillofacial surgery. Furthermore, the tensile property of the PEEK/15 vol% nHA–1.9 vol% nHA nanocomposite compared favorably with that of human cortical bones. The results of biomineralization, alkaline phosphatase (ALP), 3-(4,5-dimethylthiazol-2-yl)-2,5-diphenyltetrazolium bromide (MTT) and 2-(4-iodophenyl)-3-(4-nitrophenyl)-5-(2,4-disulfophenyl)-2*H*-tetrazolium (WST-1) assays also showed that the PEEK/15 vol% nHA and PEEK/15 vol% nHA–1.9 vol% CNF nanocomposites exhibited excellent bioactivity and biocompatibility. The ALP assay showed good activity of osteoblast cells on the composite specimens with high nHA content. Moreover, CNF addition further increased the ALP activity of PEEK/15 vol% nHA nanocomposites. The PEEK/15 vol% nHA–1.9 vol% CNF composite, with enhanced tensile strength and excellent biocompatibility, shows large potential for load-bearing implant applications.

Received 22nd October 2015
Accepted 1st February 2016

DOI: 10.1039/c5ra22134j

www.rsc.org/advances

Introduction

In recent years, there has been a substantial increase in the number of accidents in the workplace, road traffic and from sports activities. These result in unavoidable bone injuries. Furthermore, the number of aging population has also increased dramatically in developed and undeveloped countries.[1,2] Elderly people have a higher risk of bone fractures that imposes significant social and economic burdens to our society. Autografts removed from the bones of patients and allografts taken from cadavers are traditionally used for replacing bone tissue defects. Both autografts and allografts have many drawbacks, including limited availability, immunological rejection and possible disease transmission.[3] Therefore, there is a high demand for artificial implants with excellent biocompatibility for orthopedics. Metallic alloys are widely used for making bone fixation devices and implants. Metallic alloys offer beneficial advantages such as high mechanical flexibility due to their superior ductility and toughness.[4]

Metallic materials, such as stainless steel, Co–Cr and Ti–6Al–4V alloys, have been used extensively for fabricating load-bearing hip implants. However, these implants undergo corrosion upon exposure to human body fluids. Released ions from the implants can cause allergic reactions, inflammation and

[a]*Department of Physics and Materials Science, City University of Hong Kong, Tat Chee Avenue, Kowloon, Hong Kong. E-mail: aptjong@cityu.edu.hk*

[b]*Department of Materials Science and Engineering, South University of Science and Technology of China, Shenzhen, China*

[c]*Department of Orthopedics and Traumatology, Li Ka Shing Faculty of Medicine, The University of Hong Kong, Hong Kong*

cytotoxicity.[5–9] The presence of 0.9% NaCl in body fluid can also induce pitting. The chloride ion attacks protective passivation films formed on metallic surfaces.[10,11] The movement of an artificial hip prostheses produces metallic wear debris that can lead to the secretion of cytokines by macrophages.[12] These cytokines then recruit more immune cells to the site of inflammation and form giant cells.[13] Metallic implants also experience a stress shielding effect due to their elastic modulus exceeds far more than that of cortical bones.

Polymers are attractive materials for fabricating bone implants because of their good processability and lightness in weight.[14–19] Polyetheretherketone (PEEK) exhibits a high melting temperature (343 °C), high temperature durability, excellent radiation stability and high Young's modulus (3.8 GPa).[20] Accordingly, PEEK has been increasingly used for making trauma, orthopedic and spinal fixation devices.[21–23] From a review study on recent biomedical applications of PEEK and its composites reinforced with carbon fibers (CFs), PEEK is currently used for fabricating cervical spine cages and lumbar spinal fusions, whereas PEEK/CF composites are employed for acetabular cup bearing components in hip and knee implants.[24] In addition, PEEK has also recently found application in making custom implants for craniofacial surgery.[25] PEEK is bioinert, thus it inhibits protein adsorption and cell adhesion.[26,27] Its biocompatibility can be improved either *via* surface modifications[28,29] or by adding bioactive hydroxyapatite (HA) fillers in the form of whiskers and particulates.[30–34] Abu Bakar *et al.* incorporated large HA microparticulates (mHA) into PEEK.[32,33] They reported that the tensile modulus of the composites increases, whereas the tensile strength decreases with increasing filler content. The poor interfacial bonding causes de-cohesion of mHA particles from the PEEK matrix.

In general, large HA particulates often fracture into small fragments during tensile loading. Large filler loading levels often lead to poor processability of polymer composites.[34–38] Recent development in nanotechnology allows scientists to synthesize various nanomaterials with enhanced chemical, physical and mechanical properties.[39–41] In particular, ceramic nanomaterials with excellent biocompatibility show large potential for use in the biomedical sector.[42–50] Nanotechnology opens new opportunities for developing novel biomaterials that can mimic and reinforce bone tissues.[51–53] Furthermore, only low loading levels of nano-fillers are needed for reinforcing polymers.[54–57]

Bone tissue is a biocomposite consisting of a collagen matrix and HA nanorods (nHA) in which cortical bone has an elastic modulus of 7 GPa.[58] Synthetic nHA promotes protein adsorption and osteoblast growth, leading to osseointegration.[45] Therefore, nHA/polymer composites have recently been studied for their clinical use in load-bearing hip prostheses and bone tissue engineering.[59–62] In a previous study, we have prepared PEEK composites using nHA and PEEK powders *via* powder processing and furnace sintering.[59] In that process, both nHA and PEEK powders are first mechanically mixed followed by furnace sintering. However, the powder processing technique is inadequate to make PEEK nanocomposites with optimal mechanical properties. It requires high filler loading, *i.e.* 50 wt% nHA (29.2 vol% nHA) to achieve an elastic modulus of 6.73 GPa.[59] Recently, Wang *et al.* fabricated PEEK/nHA nanocomposites by mechanical mixing PEEK powders with nHA rods followed by injection molding.[63] They reported that the fracture strength of all nanocomposites is poorer than that of pure PEEK. The poor performance of such PEEK/nHA composites resulted from the use of PEEK powders. In this study, we intend to employ nHA and molded-grade PEEK pellets to fabricate PEEK/nHA biocomposites using injection molding. To further enhance the mechanical performance of PEEK/nHA nanocomposites, carbon nanofibers (CNFs) are simultaneously added to the PEEK/nHA composites. Carbon nanofibers generally exhibit good biocompatibility,[64,65] and are very effective for reinforcing PEEK.[66] Thus, may be feasible to produce biocompatible PEEK/nHA–CNF composites with good mechanical properties commercially in bulk quantities using the injection molding process.

Experimental

Materials

Nano-hydroxyapatite rods were purchased from Nanjing Emperor Nanomaterial (China). A transmission electron microscopy (TEM; Philips CM20) image of nHAs is shown in Fig. 1. PEEK-Optima pellets and carbon nanofibers were bought from Invibio Company and Nanostructured & Amorphous Materials Inc. (USA), respectively. Inorganic reagents, such as $CaCl_2$, NaCl, KCl, KH_2PO_4, $NaHPO_4$, $NaHCO_3$ and Na_2SO_4, were supplied by Sigma-Aldrich Inc. (U.S.A.). They were used directly without further purification. PEEK pellets and nHA were dried in an oven at 55 °C overnight prior to melt-compounding.

Preparation of nanocomposites

The chemical compositions of binary nHA/PEEK nanocomposites were listed in Table 1. Carbon nanofibers were only added to nHA/PEEK composites with high filler content to create hybrid composites. The compositions of all composite

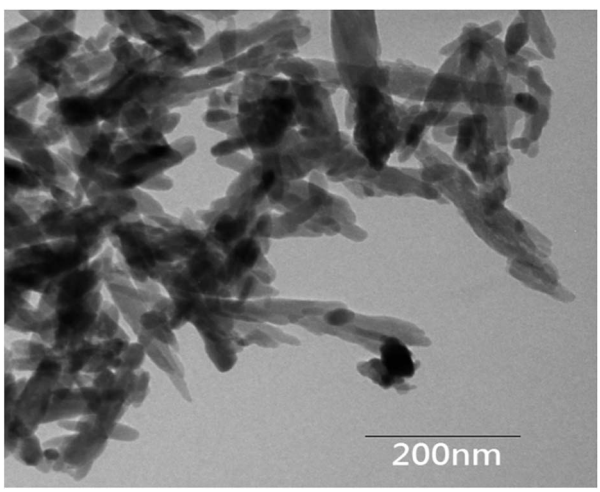

Fig. 1 TEM micrograph of HA nanorods.

Table 1 The compositions of PEEK/nHA and PEEK/nHA–CNF nanocomposites

	nHA		CNF	
Specimens	wt%	vol%	wt%	vol%
PEEK	0	0	0	0
PEEK/4.4 vol% nHA	10	4.4	0	0
PEEK/9.3 vol% nHA	20	9.3	0	0
PEEK/15 vol% nHA	30	15	0	0
PEEK/21.5 vol% nHA	40	21.5	0	0
PEEK/9.3 vol% nHA–1.6 vol% CNF	20	9.3	2	1.6
PEEK/15 vol% nHA–1.9 vol% CNF	30	15	2	1.9

samples in this article were expressed in volume percentage. Dried PEEK pellets and nHA were initially compounded in a Brabender compounder at a screw rotation speed of 30 rpm for 45 min. The mixing temperatures of Brabender from hopper to extrusion die were maintained at 360–380–390–395–380–360 °C. The extrudates were cut into small pellets by a pelletizer and fed into the Brabender again for a second mixing under the same conditions to achieve a homogeneous dispersion of nanofillers in the polymer matrix. The extruded products were pelletized again, dried overnight in an oven and finally fed into an injection molder (Toyo TI-50H) to produce dog-bone tensile bars and circular disks. The disks were mainly used for cell culture, cell viability and alkaline phosphatase activity measurements.

Material characterization and tensile tests

The morphological features of the as-fabricated composite specimens, and adhered osteoblasts on specimen surfaces, were examined in a SEM (Jeol JSM 820). The composites were dipped in liquid nitrogen and then fractured by a hammer. The fractured surfaces were then coated with a thin carbon film. Tensile tests were performed at room temperature using an Instron tester (model 5567) at a crosshead speed of 1 mm min^{-1}. The elastic modulus of PEEK-based composites was determined from the linear region of stress–strain curves. Five samples of each composition were tested, and the average values were reported.

Thermogravimetric analysis

Thermogravimetric experiments were carried out using the TGA1 STARe system (Mettler Toledo AG, Switzerland) in a nitrogen atmosphere from 50 to 800 °C at 10 °C min^{-1}. The temperatures at 10% weight loss ($T_{10\%}$) and 30% weight loss ($T_{30\%}$) were determined from the weight loss *vs.* temperature curves.

Cell culture

Human osteoblasts (Saos-2) were cultured in Dulbecco's Modified Eagle's Medium (DMEM) supplemented with 10% fetal bovine serum, penicillin and streptomycin. Injection molded disks were sliced into small rectangles for cell seeding and growth measurements. These samples were ground with SiC papers of different grades, followed by rinsing with 70% ethanol and phosphate buffer saline (PBS) solutions. Rinsed samples were placed in a 96-well plate; a cell suspension was pipetted at 10^4 cells per well. The plate was placed inside an incubator under a humidified atmosphere of 5% CO_2/95% air at 37 °C for 1 and 3 days. The culture medium was changed every two days. Following the incubation, the samples were washed with phosphate-buffered saline (PBS), fixed with 10% formaldehyde and dehydrated in a graded series of ethanol baths. Dehydrated cells were critical point dried and sputter-deposited with gold in preparation for SEM examination.

Cell viability

Osteoblastic cell viability was assessed using 3-(4,5-dimethylthiazol-2-yl)-2,5-diphenyltetrazolium bromide (MTT), and 2-(4-iodophenyl)-3-(4-nitrophenyl)-5-(2,4-disulfophenyl)-2*H*-tetrazolium (WST-1) assays. A suspension with 10^4 cells was seeded in each well (96-well plate) containing test samples (number of specimens, $n = 5$). The plate was incubated in a humidified atmosphere of 5% carbon dioxide in air at 37 °C for 3, 7 and 10 days. The culture medium was refreshed every three days. At days 3, 7 or 10, the medium was aspirated. Then, 10 μL of MTT solution (5 mg MTT : 1 mL DMEM) was added to each well and incubated for 4 h at 37 °C. In the test process, the tetrazolium ring of MTT salt was cleaved by mitochondrial enzymes, *i.e.* succinic dehydrogenase from viable osteoblasts, forming insoluble formazan crystals. MTT formazan is insoluble in water, thus, an organic solvent was needed to solubilize the crystals. The formazan was dissolved in 10% sodium dodecyl sulfate (SDS)/0.01 M hydrochloric acid (100 μL). The absorbance of dissolved formazan was measured at a wavelength of 570 nm using a multimode detector (Beckman Coulter DTX 880), with a reference wavelength of 640 nm. The results were expressed in terms of mean ± standard deviation (SD). MTT tests were repeated at least twice.

For the WST-1 assay, the samples ($n \geq 3$) were first cultured with osteoblasts at 37 °C for 3, 7 and 10 days, respectively. After cell culturing for every prescribed time period, tetrazolium salt was added to each well followed by incubation for 4 h at 37 °C. The cleaved tetrazolium product was water soluble, thus eliminating the solubilization step as required for the MTT assay. The amount of formazan formed was directly proportional to the number of metabolically active cells in the culture. The amount of water-soluble formazan was quantified by the absorbance at 450 nm. WST-1 tests were repeated at least twice. Statistical significance was assessed by the Student's *t*-test, with a significance level of $p < 0.05$ as compared to pure PEEK.

Alkaline phosphatase activity

Alkaline phosphatase (ALP) is an enzyme secreted by osteoblasts during osteogenesis and acts as the marker for their differentiation. The ALP activity of each sample (number of specimens, $n = 5$) was assessed by a colorimetric assay kit (no. 2900-500, Stanbio Laboratory, Boerne, Texas) according to

the manufacturer's instructions. The kit employed colorless 4-nitrophenyl phosphate as a substrate. The enzyme ALP of the cells hydrolyzed the substrate to colored 4-nitrophenol and an inorganic phosphate. In the measurements, test samples were placed in each well of a 24-well plate. Osteoblasts were cultured on the samples for 3, 7 and 14 days. The culture medium was changed every three days. At selected days 3, 7 or 14, the cells were rinsed with PBS, and lysed with 0.1% Triton X-100 at 4 °C for 30 min. The cell lysates were then centrifuged at 4 °C followed by placing 10 μL of the supernatant of each sample in a 96-well plate. Finally, *p*-nitrophenyl phosphate was added to the plate. The absorbance of *p*-nitrophenol formed was measured using a spectrophotometer (Beckman Coulter DTX 880) at 405 nm. The rate at which *p*-nitrophenol formed was directly proportional to ALP activity. The ALP activity was normalized to the DNA content of the samples. DNA standard (calf thymus DNA, Ultrapure D-4764; Sigma Aldrich) and Hoechst 33258 dye (Sigma Aldrich) were used in the tests. Hoechst 33258 nucleic acid dye emitted blue fluorescence at 465 nm when bound to double-stranded DNA.

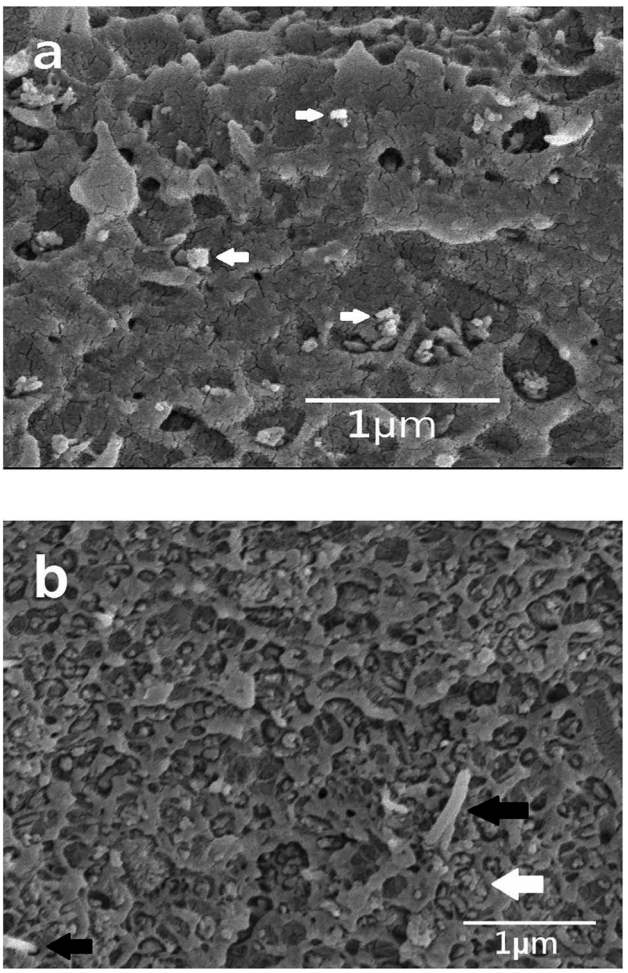

Fig. 2 SEM micrographs showing fracture surfaces of (a) PEEK/4.4% nHA and (b) PEEK/15% nHA–1.9% CNF nanocomposites. Black arrow: CNF; white arrow: nHA.

Biomineralization test

The PEEK-based nanocomposites were immersed in a simulated body fluid (SBF) solution at 37 °C for 21 days for assessing their bioactivity. This solution was prepared according to the corrected Kokubo protocol by dissolving the required amounts of reagent grade chemicals, including NaCl, $NaHCO_3$, KCl, $K_2HPO_4 \cdot 3H_2O$, $MgCl_2 \cdot 6H_2O$, $CaCl_2 \cdot 2H_2O$ and Na_2SO_4, into distilled water to obtain desired ion concentrations: Na^+ (142 mM), K^+ (5 mM), Ca^{2+} (2.5 mM), Mg^{2+} (1.5 mM), Cl^- (147.8 mM), HCO_3^- (4.2 mM), HPO_4^- (1 mM) and SO_4^{2-} (0.5 mM). The pH value of the solution was adjusted to 7.4 using tris-(hydroxymethyl)-aminomethane and 1 M HCl at 37 °C.[67,68] After immersion, the specimens were removed from the solution, rinsed with distilled water, dried, and then examined by SEM as well as by X-ray diffraction (XRD; Bruker, USA) under CuKα radiation at 30 kV.

Results and discussion

Morphology

Fig. 2a shows the SEM image of the PEEK/4.4 vol% nHA nanocomposite. It can be observed that the nHA fillers are dispersed uniformly in the polymer matrix. The polymer matrix is quite ductile as characterized by the presence of a rough surface. By increasing the nHA content to 15 vol%, most nHA fillers are still dispersed homogeneously, but a few of the nHA fillers tended to aggregate to form small agglomerates. For the PEEK/15 vol% nHA–1.9 vol% CNF composite, CNF fillers can be readily observed in Fig. 2b. As is widely recognized, polymer

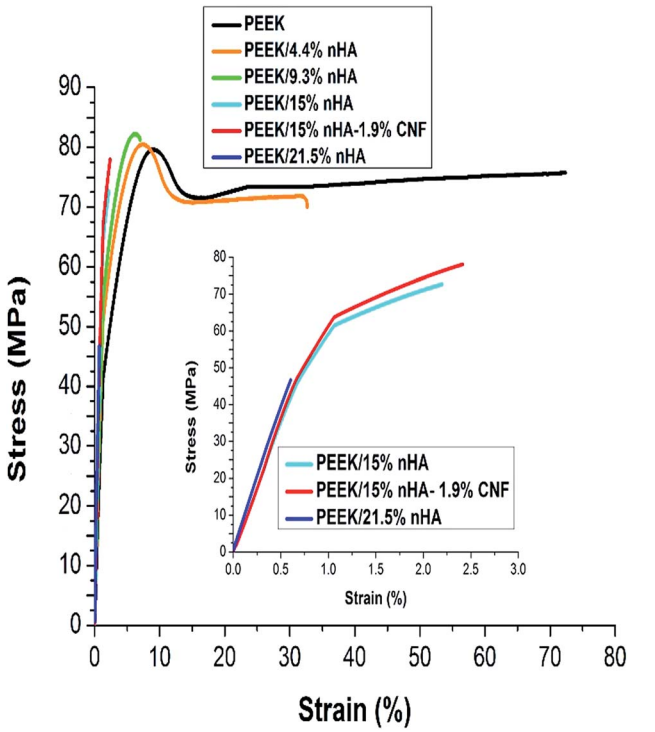

Fig. 3 Stress–strain curves of pure PEEK, PEEK/nHA and PEEK/nHA–CNF nanocomposites.

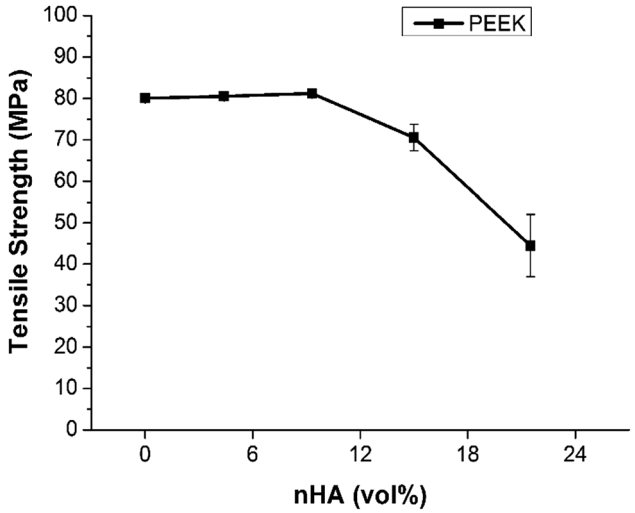

Fig. 4 Tensile strength *versus* nHA volume content for PEEK/nHA nanocomposites.

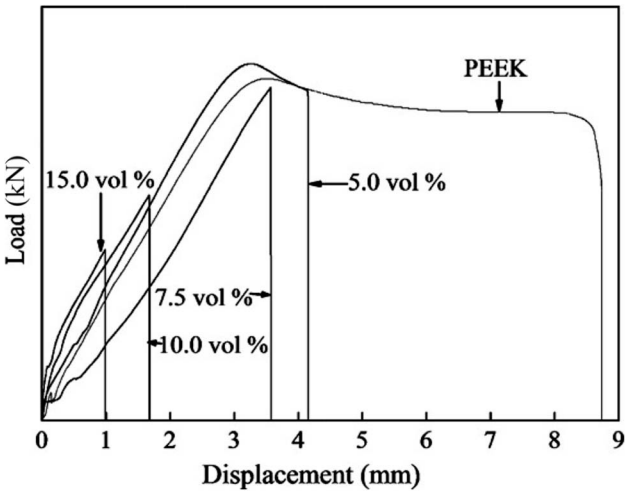

Fig. 5 Load–displacement curves of pure PEEK and PEEK/nHA nanocomposites prepared by mechanical mixing PEEK powders with nHA followed by injection molding.[63]

nanocomposites are generally reinforced with very low loading levels of fillers (*e.g.* 0.2–2 vol%) to achieve the desired chemical, physical or mechanical properties. However, polymer nanocomposites for bone implant applications require the additions of higher nHA loadings because the polymeric matrix is bioinert. Such nHA fillers can anchor osteoblasts and promote their growth on the surfaces of polymer nanocomposites. It should be noted that the nHA filler content of PEEK/nHA nanocomposites are much lower than the mHA loadings in conventional PEEK/mHA micro-composites.

Mechanical properties

Fig. 3 shows the stress–strain curves of pure PEEK, PEEK/nHA and PEEK/nHA–CNF nanocomposites. The nHA additions exhibit a beneficial effect in enhancing the elastic modulus of PEEK at the expense of tensile ductility. Furthermore, the tensile strength of PEEK/nHA nanocomposites increases slightly with nHA content up to 9.3 vol%; therefore, it decreases with increasing nHA content (Fig. 4). Thus, 4.4–9.3 vol% nHA fillers can provide mechanical interlocking with the PEEK matrix, thereby reinforcing the polymer matrix. On the contrary, the tensile strength of PEEK/nHA nanocomposites as reported by Wang *et al.* (Fig. 5) is lower than that of pure PEEK, and falls rapidly with increasing filler content.[63] Such tensile results indicate the poor load-bearing capacity of the nanocomposites. The poor performance of their PEEK/nHA composites is attributed to the use of PEEK powders rather than injection molded PEEK pellets. PEEK powders are unsuitable for injection molding purposes for fabricating nanocomposites. Furthermore, Wang *et al.* did not employ an extensometer to measure tensile strain of the specimens during tensile testing. As known, Young's modulus of a material is determined from the linear slope of stress–strain curves and not from the linear slope of the load–displacement curves. From Hooke's law, stress varies linearly with elastic modulus and strain in the elastic region.[69] To measure strain, an extensometer is attached to the gauge length of the tensile specimen. Therefore, Young's modulus is determined as the change in stress divided by change in strain in the linear portion of the stress–strain curve.[70] Therefore, the elastic modulus of their PEEK and PEEK/nHA composites cannot be determined from the load–displacement curves, as shown in Fig. 5.

Fig. 6a shows the variation of elastic modulus with nHA content for PEEK/nHA nanocomposites. The elongation *vs.* nHA volume content plot of these nanocomposites is depicted in Fig. 6b. It can be observed that the stiffness of PEEK/nHA nanocomposites increases continuously with increasing nHA content. At 21.5 vol% nHA loading, the stiffness of the PEEK/nHA composite reaches 7.85 GPa and exceeds the lower limit of cortical bone with a value of 7 GPa.[58] Despite the high stiffness of the PEEK/21.5% nHA nanocomposite, its tensile strength (44.51 MPa) and elongation at break (0.69%) are lower than those of human cortical bone. The tensile stress and fracture strain of cortical bone are 50 MPa and 1%, respectively. The PEEK/21.5% nHA nanocomposite with a tensile strain of 0.69% is brittle, as expected, and unlikely to be used as the material for making bone implants. In this respect, particular attention is paid to the tensile behavior of the PEEK/15% nHA nanocomposite with tensile strain of 2.71% and tensile stress of 70.56 MPa because both tensile values are higher than those of cortical bone. The elastic modulus of the PEEK/15% nHA nanocomposite is 6.2 GPa (Fig. 6). By adding 1.9 vol% CNF to the PEEK/15% nHA nanocomposite, the modulus increases to 6.54 GPa, whereas the tensile stress and fracture strain also increase to 71.67 MPa and 2.83%, respectively.

As aforementioned, metallic implants have many drawbacks for orthopedic applications, including corrosion problem, cytotoxicity of metallic ions and stress shielding effect. In the latter case, the extremely large elastic modulus of metallic implants (*e.g.* Ti–6Al-4V alloy (110 GPa) and Co–Cr alloy (240 GPa)) can lead to a stress shielding effect, causing bone loss and eventual implant loosening. Stress shielding in the femur

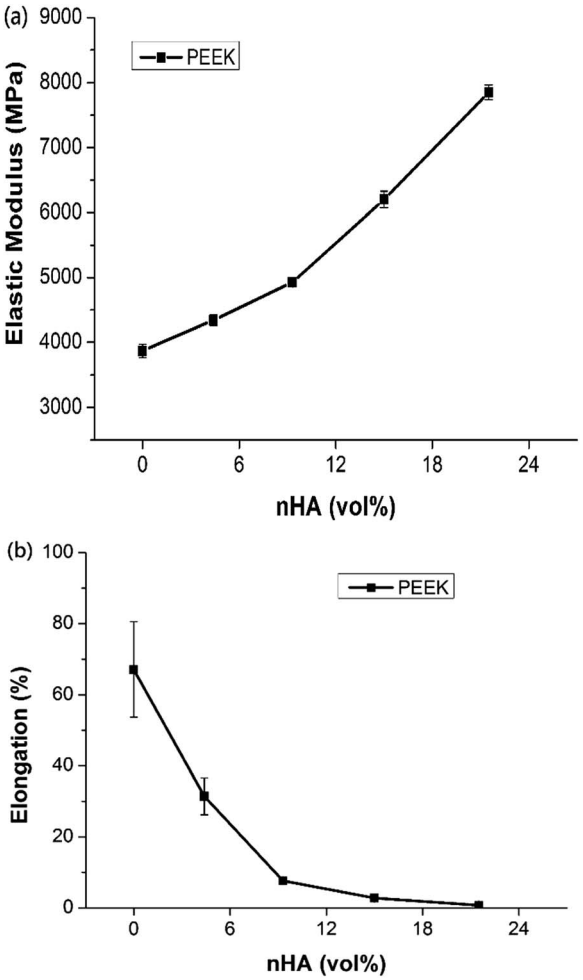

Fig. 6 (a) Elastic modulus as a function of filler content, and (b) elongation at break *vs.* nHA content for PEEK/nHA nanocomposites.

occurs when some of the loads are taken by the prosthesis and shielded from going to the bone. As a consequence, polymeric materials with low elastic modulus appear to be attractive for use in orthopedics. High-density polyethylene (HDPE) reinforced with 40 vol% mHA particles (HAPEX) has been developed commercially for biomedical applications. The elastic modulus, tensile stress and fracture strain of the HAPEX composite are 4.29 GPa, 20.67 MPa and 2.6%, respectively.[71] However, the tensile strength of HAPEX (20.67 MPa) is far below the strength of cortical bone (50 MPa). Thus HAPEX can only be used as non-load bearing biocomposites for maxillofacial surgery, orbital floor prosthesis and middle ear implants.[72] In the present study, the PEEK/9.3 vol% nHA nanocomposite with a favorable mechanical performance, *i.e.* elastic modulus of 4.92 GPa, tensile stress of 81.23 MPa and fracture strain of 7.62%, can replace HAPEX for use in maxillofacial surgery. Moreover, its PEEK matrix with the high melting temperature of 343 °C, excellent radiation stability and low moisture absorption, provides high levels of resistance for sterilization.[20] Therefore, the molecular chains of PEEK do not degrade either during autoclave sterilization or gamma-ray radiation treatment.

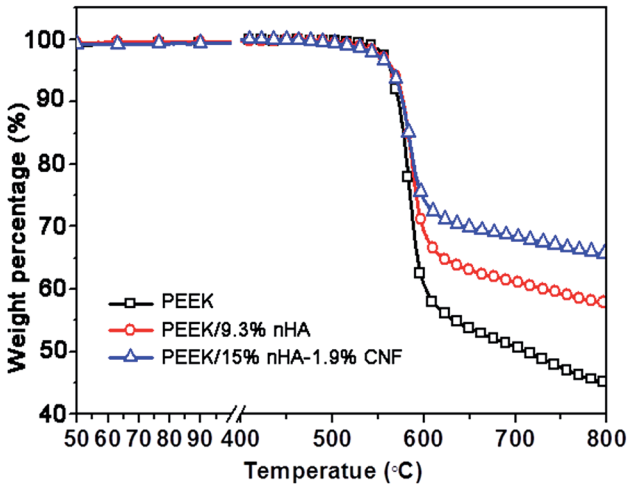

Fig. 7 TGA curves of pure PEEK, PEEK/9.3 vol% nHA and PEEK/15 vol% nHA–1.9 vol% CNF nanocomposites.

Medical devices must be sterilized to prevent the introduction of pathogens into the body. On the contrary, polyethylene is unable to withstand high temperature and pressure conditions during the sterilization process. Irradiation of polyethylene results in the scission of molecular chains and the formation of degradation products.[73] In this study, the PEEK/15 vol% nHA–1.9 vol% CNF bio-nanocomposite with good mechanical performance shows potential for use as a material for load-bearing implants in orthopedics.

Thermal stability

TGA measurements have been used to provide the substantiate evidence for high thermal stability of PEEK and its nanocomposites (Fig. 7). Highly stable PEEK can prevent thermal degradation during sterilization. TGA results of representative specimens are listed in Table 2. Apparently, PEEK exhibits very high $T_{10\%}$ and $T_{30\%}$ decomposition temperatures, demonstrating its high thermal stability. The increase of thermal decomposition temperature is often regarded as an indicator for an improvement in thermal stability. The decomposition temperature of PEEK is considerably higher than that of HDPE (335 °C).[74] Furthermore, the 9.3% nHA addition increases the $T_{30\%}$ of PEEK from 588 to 598 °C. Hybridizing CNF with nHA can further increase the $T_{30\%}$ value of PEEK to 645 °C. The excellent thermal properties of PEEK are attributed to the stability of its aromatic backbone. PEEK consists of bulky molecules that cannot volatilize easily. Therefore, weight loss is not observed until the thermal scission products of PEEK are

Table 2 TGA results of PEEK and representative composites

Specimen	$T_{10\%}$ (°C)	$T_{30\%}$ (°C)
PEEK	572	588
PEEK/9.3% nHA	577	598
PEEK/15% nHA–1.9% CNF	577	645

volatilized. Thermal degradation of PEEK involves chain scissions of the ether and ketone bonds, giving rise to low molecular volatiles such as diphenyl ether and phenol at high temperatures.[75,76]

From Fig. 7, PEEK decomposes more intensely above 600 °C, resulting in the volatilization of around 45% of the polymer mass. In the presence of 9.3% nHA, large mass loss also occurs above 600 °C, causing volatilization of about 35% of the polymer mass when compared with pure PEEK. The mass loss can be further decreased to 30% by incorporating 15% nHA and 1.9% CNF into PEEK. This result implies that very low CNF loading markedly improves the thermal stability of PEEK. Carbon nanofibers can generally be classified as multi-walled carbon nanotubes with larger diameters (less than 500 nm). The beneficial effect of carbonaceous nanomaterials such as carbon nanotubes in enhancing thermal stability of polymers has been

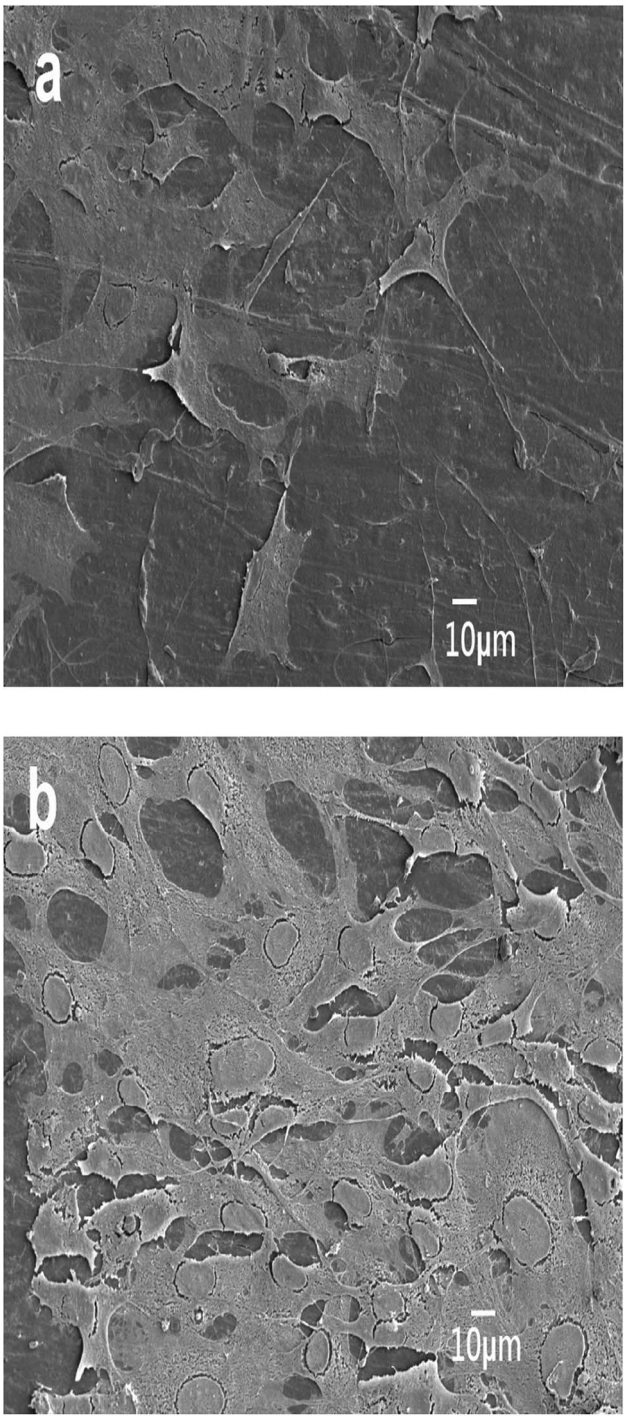

Fig. 8 SEM micrographs of PEEK/9.3% nHA nanocomposite cultured with osteoblasts for (a) 1 and (b) 3 days.

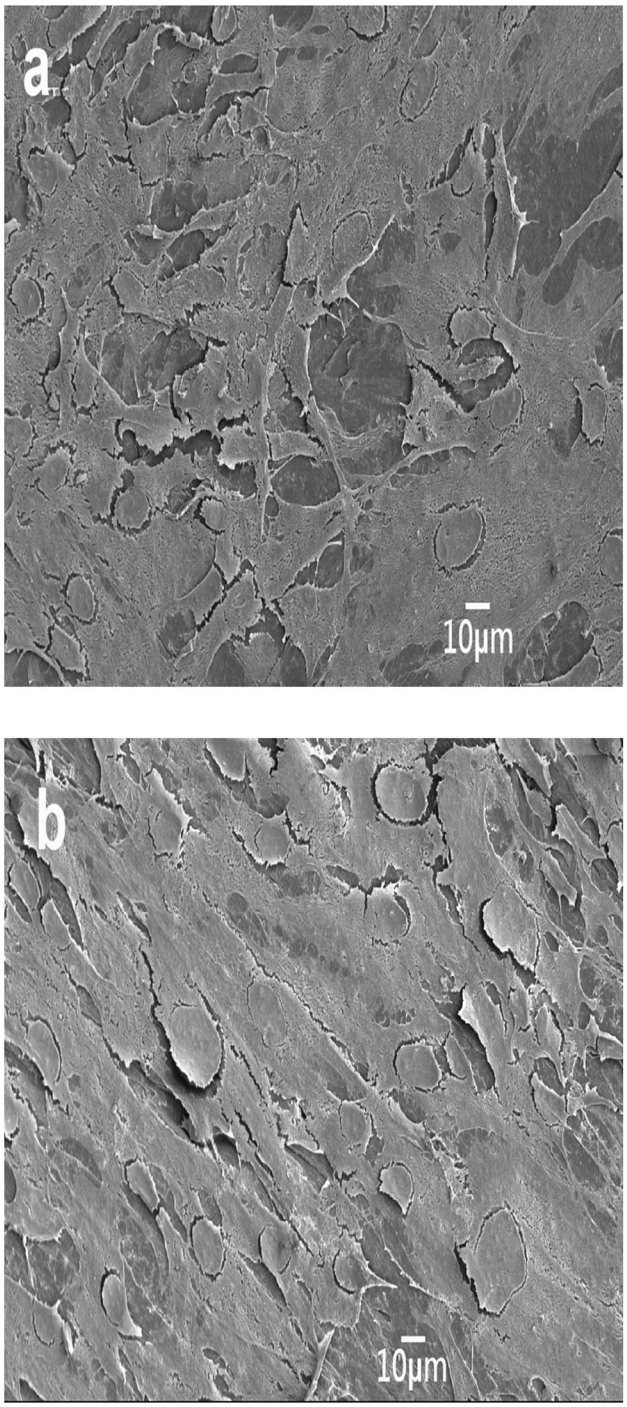

Fig. 9 SEM micrographs of PEEK/15% nHA nanocomposite cultured with osteoblasts for (a) 1 and (b) 3 days.

reported in the literature. The stabilization effect of carbon nanotubes on the polymer is explained by a barrier effect of the nanotubes that hinder the diffusion of the degradation products from the bulk of the polymer onto the gas phase.[77]

Cellular adhesion and viability

The adherence of cells to the material surface is evaluated through SEM imaging. Fig. 8a and b and 9a and b are the SEM micrographs of PEEK/9.3% nHA and PEEK/15% HA nanocomposites cultured with osteoblasts for 1 and 3 days, respectively. The cells anchor tightly on the surfaces of these composite specimens after cultivation for 1 day. The cells then grow and spread flatly on the surfaces such that many neighbor cells join with each other through cytoplasmic extension after 3 days of cultivation. Consequently, entire surface of the PEEK/15% HA nanocomposite is covered with osteoblasts (Fig. 9b). Bioinert PEEK does not promote osteoblastic adhesion and proliferation. The nHA fillers serve as effective sites for the adhesion and growth of osteoblasts. SEM images of cell-cultured nanocomposites at day 1 and 3 are presented herein to display the difference of cell coverage on the specimen surfaces. Lower cell attachment is observed at day 1, whereas nearly or full cell coverage is observed at day 3. Above day 3, entire surfaces are covered with osteoblasts.

Fig. 10 shows the MTT results for PEEK and its nanocomposites. A dramatic increase in cell viability can be observed on PEEK/nHA nanocomposites at every test time period compared to the PEEK control. Furthermore, the addition of CNF to PEEK/9.3% nHA and PEEK/15% nHA composites does not impair the viability of osteoblasts. In contrast, a slight increase in cell viability is found for the PEEK/9.3% nHA–1.6% CNF and PEEK/15% nHA–1.9% CNF composites. Comparing with single-walled and multi-walled carbon nanotubes, carbon nanofibers have been reported to have higher cell viability.[64] Price *et al.* also reported that carbon nanofibers promote osteoblast adhesion.[65] As aforementioned, the MTT assay requires an additional solubilization step to dissolve colored formazan crystals resulting from the metabolic activity of mitochondria. Such formazan crystals do not dissolve completely in an organic solvent, particularly in the presence of carbonaceous nanomaterials such as carbon nanotubes.[78] Those undissolved crystals in a solvent can lead to low colorimetric results in the spectrophotometric measurement, resulting in low cell viability. In contrast, the WST-1 assay obtains water soluble formazan and would not form insoluble clusters such as MTT. Therefore, the WST-1 assay yields more reliable results for cell viability. Fig. 11 shows the cell viability measured by the WST-1 assay for PEEK-based nanocomposites. It is evident that the WST-1 assay obtains considerably higher cell viability than the MTT assay. From Fig. 10 and 11, the MTT and WST-1 tests cover 3, 7 and 10 days. At day 3, the results show low cell viability. Additional 7 and 10 days are needed for testing cell viability to achieve higher cell viability. In this respect, the difference in cell viability of each sample becomes more apparent.

It is worth noting that nanomaterials may induce a cytotoxic effect on biological cells. Grabinski *et al.* indicated that cytotoxicity of carbon materials is dependent on their dimensions.[64] Carbon fibers (10 μm diameter) and CNF (100 nm diameter) did not significantly affect the viability of mouse keratinocytes, whereas multi-walled carbon nanotubes (10 nm diameter) reduced cell viability greatly. The cytotoxic action of carbon nanotubes in general is caused by suspending them independently in the cell culture medium. As such, independent carbon nanoparticles can penetrate cell membranes and reside inside the cytoplasm.[79,80] Our previous study showed that the polymer matrix of nanocomposites is an effective material for encapsulating CNFs.[81] Therefore, CNFs embedded firmly in the polymer matrix of nanocomposites act as excellent substrates for the adhesion, growth and viability of osteoblasts.

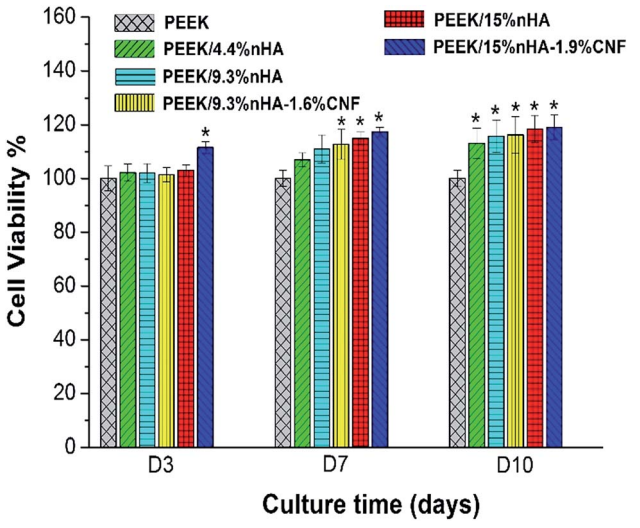

Fig. 10 MTT assay results showing cell viability of human osteoblasts (Saos-2) grown on PEEK and its nanocomposites for 3, 7 and 10 days. * represents $p < 0.05$.

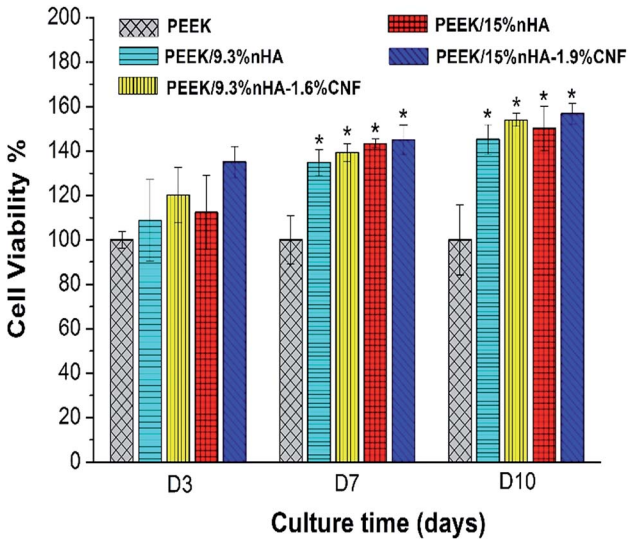

Fig. 11 WST-1 assay results showing cell viability of human osteoblasts (Saos-2) grown on PEEK and its nanocomposites for 3, 7 and 10 days. * represents $p < 0.05$.

Alkaline phosphatase activity

Alkaline phosphatase is an important component in hard tissue formation and is highly expressed in mineralized tissue cells. Proliferating osteoblasts show alkaline phosphatase activity, and this is greatly enhanced during *in vitro* bone formation. Alkaline phosphatase catalyzes hydrolysis of phosphate esters in alkaline buffer and produces phenol and inorganic phosphate. Fig. 12 shows the ALP activity of PEEK and its nanocomposites at days 3, 7 and 14. The ALP enzymatic assay results reveal good ALP activity level of osteoblasts on the PEEK/nHA composites at day 14. In particular, ALP activity increases with increasing nHA content of the composites. This is because nHA fillers promote osteoblastic cell adhesion and differentiation. In addition, synthetic nHA exhibits excellent osteoconductivity and biocompatibility. As recognized, osteoblastic cell differentiation plays an important role in osteogenesis, or bone formation, at early stages.[82] ALP is an enzyme produced by cells that participate in bone tissue mineralization through the deposition of minerals on the extracellular matrix (ECM) molecules.

From the osteoblastic differentiation model proposed by Stein and Lian,[83] bone cells proliferate greatly up to 7–14 days and then begin to secrete ECM proteins and produce ALP differentiation markers for matrix mineralization. Upon completion of adhesion and proliferation, osteoblastic differentiation is then initiated to secrete proteins, minerals and collagens for bone tissue mineralization. It is interesting to observe that the ALP activity of the PEEK/15% nHA nanocomposite can be increased by adding CNF. In a previous study, the hybridization of nHA filler with CNF promotes osteoblastic adhesion and proliferation.[81] CNFs and multi-walled carbon nanotubes have been reported to enhance osteoblastic adhesion and differentiation by promoting protein–material interactions.[65,84,85] Elias *et al.* demonstrated that osteoblast adhesion, proliferation, alkaline phosphatase activity, and ECM secretion on carbon nanofibers increases with decreasing fiber diameter in the range of 60–200 nm.[84]

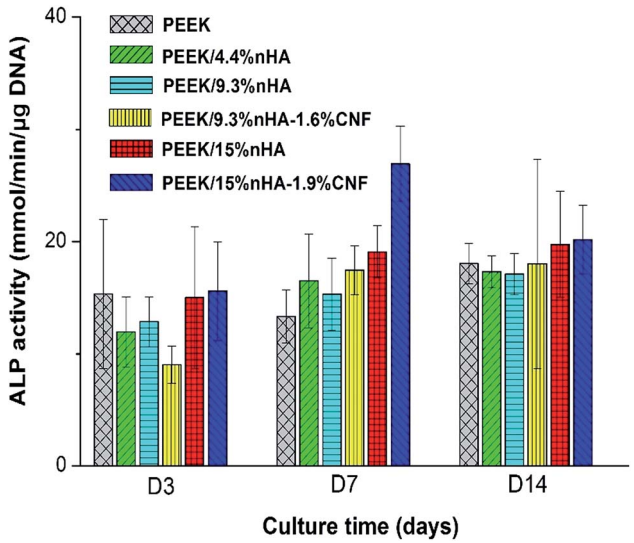

Fig. 12 ALP activity normalized to DNA content of human osteoblasts (Saos-2) grown on PEEK and its nanocomposites for 3, 7, and 14 days.

Bioactivity

SBF is a solution that mimics the inorganic ion composition of human plasma. Apatite-forming ability is one of the major mechanisms of chemical bioactivity.[86] By performing SBF immersion, the apatite layer forming ability, or bioactivity, of our PEEK/nHA and PEEK/nHA–CNF nanocomposites can be assessed. The SBF test is widely used by researchers to evaluate the capability of test samples to form an apatite layer on their surfaces.[68,86–89] The main difference between SBF and the inorganic component of plasma is the carbonate concentration: 4.2 mM in SBF and 27 mM in plasma. The carbonate deficiency in SBF is compensated by a greater concentration of chloride

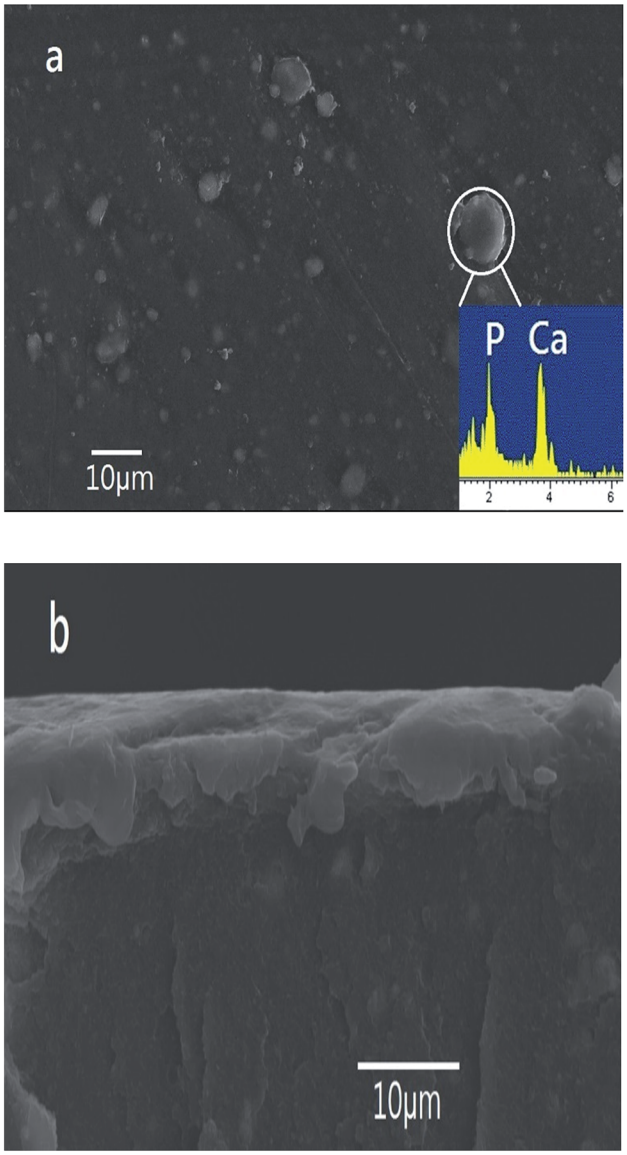

Fig. 13 (a) Plan-view and (b) cross-sectional SEM micrographs of the PEEK/9.3% nHA nanocomposite after soaking in SBF solution for 21 days.

ions, therefore the electroneutrality of solution is maintained.[68] Fig. 13a is a SEM micrograph showing the morphology of an apatite layer deposited on the surface of the PEEK/9.3% nHA nanocomposite after soaking in SBF solution for 21 days. Many globular apatite particles can be observed on the composite surface. X-ray energy dispersive spectrum (EDS) of the globular apatite reveals the presence of calcium and phosphorus. The nHA fillers act as nucleation sites for apatite deposition. The formation mechanism of apatite on the surface of nHA can be attributed to the ion exchange between nHA and the SBF solution.[90,91] The OH^- and PO_4^{3-} groups of the nHA fillers give rise to negatively charged surfaces. Thus, Ca^{2+} ions in the SBF are attracted towards the nHA of the nHA/PEEK nanocomposites. Furthermore, nHA fillers also contain Ca^{2+} ions on their surfaces. As more positive charge is built-up, PO_4^{3-} ions from the SBF are also attracted to this site, forming calcium phosphate deposits that eventually crystallize into an apatite layer.[91] A cross-sectional SEM image of the apatite layer formed on the surface of this nanocomposite is shown in Fig. 13b. Apparently, a dense apatite layer is deposited on the composite surface after soaking for 21 days. Fig. 14a and b are the SEM micrographs showing plan-view and cross-sectional images of the PEEK/15% nHA–1.9% CNF nanocomposite. The plan-view micrograph reveals the presence of more apatite nodules on the surface of this composite with higher nHA content. The nodules then form a compact and continuous layer over the surface. A similarly dense apatite layer can be observed on the surface of this nanocomposite (Fig. 14b), demonstrating its good bioactivity.

Comparing with HA fillers of micrometer dimension, the nHA fillers with a large surface area favor formation of more apatite nodules as higher Ca^{2+} ions and PO_4^{3-} groups are concentrated on their surfaces. Moreover, nHAs with a large surface area provides more nucleation sites for apatite nodules. The nucleating effect of apatite nodules increases with nHA content in the nanocomposites. Recently, Yang *et al.* reported that the incorporation of nHA into polycaprolactone (PCL) facilitates the precipitation of apatite nodules on their surface due to the enhanced dissolution of nHA and the subsequent release of Ca^{2+} ions, which favors apatite deposition.[92]

A bone-like hydroxyapatite layer generally obtains a Ca/P ratio close to 1.65, which is the value reported for bone. The Ca/P ratio values determined from the EDS profiles as shown in Fig. 13a and 14a are 1.62 and 1.65, respectively. Fig. 15 shows the XRD pattern of the mineralized layer on the surface of a representative PEEK/15% nHA nanocomposite after immersion in SBF for 21 days. The diffraction peaks of PEEK in the

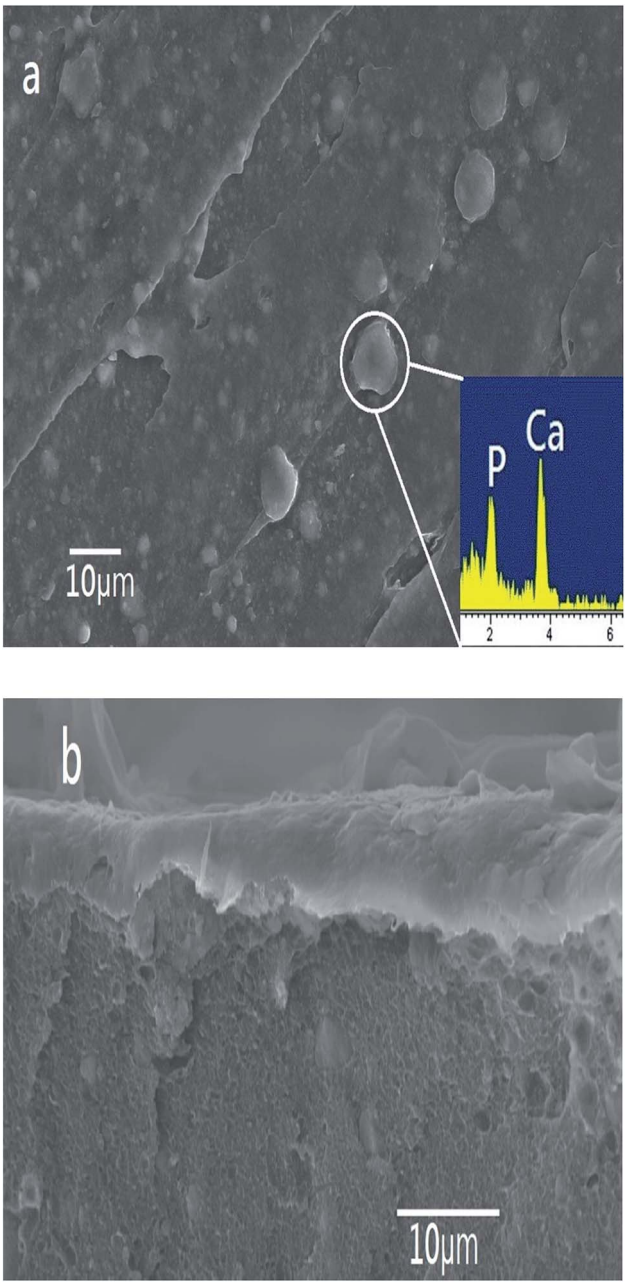

Fig. 14 (a) Plan-view and (b) cross-sectional SEM images of the PEEK/15% nHA–1.9% CNF nanocomposite after soaking in SBF solution for 21 days.

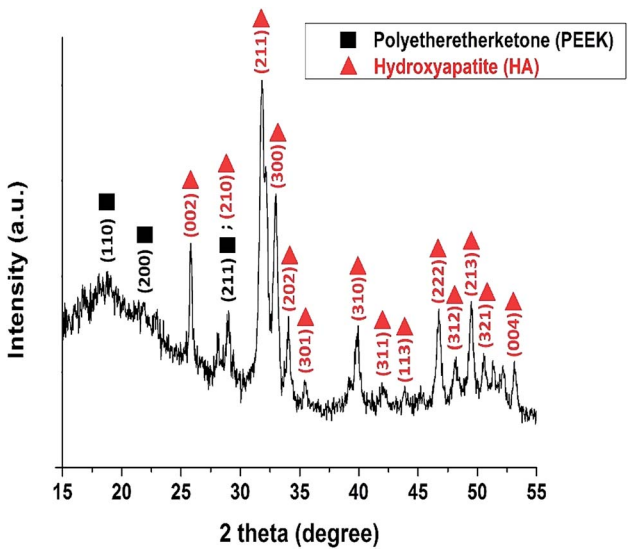

Fig. 15 XRD pattern of mineralized layer deposited on the PEEK/15% nHA nanocomposite after immersion in SBF for 21 days.

pattern are indexed.[93,94] The small thickness of the deposited layer induces PEEK peaks. In addition, nHA peaks can be readily observed in the pattern. All the nHA planes in the pattern have been indexed in accordance with the Joint Committee on Powder Diffraction Standards (JCPDS no. 09-0432) for hydroxyapatite, $Ca_{10}(PO_4)_6(OH)_2$. From these results, the mineralized layer formed on the composite surface is hydroxyapatite.

Conclusions

In this study, we presented the preparation, biochemical, mechanical and thermal characterizations of PEEK/nHA and PEEK/nHA–CNF nanocomposites for bone replacements in orthopedics. Our results showed that the PEEK/9.3% nHA nanocomposite with good mechanical, thermal and biological performances can be considered as a biomaterial for use in maxillofacial surgery. This nanocomposite exhibited higher tensile strength than a conventional HAPEX composite reinforced with 40 vol% HA micro-particles. Furthermore, tensile test results revealed that the PEEK/15% nHA–1.9% CNF nanocomposite exhibits comparable tensile properties with human cortical bones. TGA measurements showed that the incorporation of nHA filler or CNF and nHA hybrid fillers into PEEK increases the thermal stability. Hybridization of CNF with nHA fillers was found to increase the $T_{30\%}$ value of PEEK from 588 °C to 645 °C, and to effectively reduce mass loss at high temperatures. As such, thermal degradation of the PEEK hybrid nanocomposite can be avoided during sterilization treatment. Accordingly, PEEK/15% nHA–1.9% CNF nanocomposite shows high potential for use as a biomaterial for load-bearing implants.

MTT and WST-1 results demonstrated that cell viability of osteoblasts increases with increasing nHA content in the PEEK/nHA nanocomposites. In addition, a PEEK/nHA nanocomposite with high nHA content (*i.e.* 15%) exhibited higher ALP activity compared to pure PEEK. The presence of the nHA mineral phase enhanced ALP activity, an early marker of bone formation. Moreover, CNF addition further increased the ALP activity of the PEEK/15% nHA nanocomposite.

Acknowledgements

This study is supported by a Strategic Research Grant (Project No. 7004384), City University of Hong Kong, and Shenzhen Science and Technology Project Grant (JCYJ20150630145302228), China.

References

1 C. M. Aldwin and D. F. Gilmer, *Health, Illness, and Optimal Aging: Biological and Psychosocial Perspectives*, Springer, New York, 2013.
2 T. Dening and A. Thomas, *Old Age Psychiatry*, Oxford University Press, Oxford, 2nd edn, 2013.
3 A. Oryan, S. Alidadi, A. Moshiri and N. Maffulli, *J. Orthop. Surg. Res.*, 2014, **9**, 18.
4 S. Q. Wu, H. G. Zhu and S. C. Tjong, *Metall. Mater. Trans. A*, 1999, **30**, 243–248.
5 J. J. Jacobs, J. L. Gilbert and R. M. Urban, *J. Bone Jt. Surg., Am. Vol.*, 1998, **80**, 268–282.
6 N. Hallab, K. Meritt and J. J. Jacobs, *J. Bone Jt. Surg., Am. Vol.*, 2001, **83**, 428–436.
7 Y. Okazaki and E. Gatoh, *Biomaterials*, 2005, **26**, 11–21.
8 B. Scharf, C. C. Clement, V. Zolla, G. Perino, B. Yan, S. G. Elci, E. Purdue, S. Goldring, F. Macaluso, N. Cobelli, R. W. Vachet and L. Santambrogio, *Sci. Rep.*, 2014, **4**, 5729.
9 V. S. Challa, S. Mali and R. D. K. Misra, *J. Biomed. Mater. Res., Part A*, 2013, **101**, 2083–2089.
10 S. C. Tjong and E. B. Yeager, *J. Electrochem. Soc.*, 1981, **128**, 2251–2254.
11 S. C. Tjong, R. W. Hoffman and E. B. Yeager, *J. Electrochem. Soc.*, 1982, **129**, 1662–1668.
12 N. Cobelli, B. Scharf, G. M. Crisi, J. Hardin and L. Santambrogio, *Nat. Rev. Rheumatol.*, 2011, **7**, 600–608.
13 J. Pajarinen, T. H. Lin, T. Sato, Z. Yao and S. B. Goodman, *J. Mater. Chem. B*, 2014, **2**, 7094–7108.
14 S. C. Tjong and Y. Z. Meng, *Eur. Polym. J.*, 2000, **36**, 123–129.
15 Y. Z. Meng, S. C. Tjong, A. S. Hay and S. J. Wang, *J. Polym. Sci., Part A: Polym. Chem.*, 2001, **39**, 3218–3226.
16 X. H. Li, S. C. Tjong, Y. Z. Meng and Q. Zhu, *J. Polym. Sci., Part B: Polym. Phys.*, 2003, **41**, 1806–1813.
17 Y. Z. Meng and S. C. Tjong, *Polymer*, 1998, **39**, 99–107.
18 Y. Z. Meng, A. S. Hay, X. G. Jian and S. C. Tjong, *J. Appl. Polym. Sci.*, 1998, **68**, 137–143.
19 L. C. Du, Y. Z. Meng, S. J. Wang and S. C. Tjong, *J. Appl. Polym. Sci.*, 2004, **92**, 1840–1846.
20 A. M. Díez-Pascual, M. Naffakh, C. Marco, G. Ellis and M. A. Gómez-Fatou, *Prog. Mater. Sci.*, 2012, **57**, 1106–1190.
21 S. M. Kurtz and J. N. Devine, *Biomaterials*, 2007, **28**, 4845–4869.
22 E. L. Steinberg, E. Rath, A. Slaifer, O. Chechik, E. Maman and M. Salai, *J. Mech. Behav. Biomed. Mater.*, 2013, **17**, 221–228.
23 R. K. Ponnappan, H. Serhan, B. Zarda, R. Patel, T. Albert and A. R. Vaccaro, *Spine J.*, 2009, **9**, 263–267.
24 M. R. Abdullah, A. Goharian, M. R. Kadir and M. U. Wahit, *J. Biomed. Mater. Res., Part A*, 2015, **103**, 3689–3702.
25 E. Alonso-Rodriguez, J. L. Cebrián, M. J. Nieto, J. L. Del Castillo, J. Hernández-Godoy and M. Burgueno, *Journal of Cranio-Maxillofacial Surgery*, 2015, **43**, 1232–1238.
26 R. Ma, S. Tang, H. Tan, J. Qian, W. Lin, Y. Wang, C. Liu, J. Wei and T. Tang, *ACS Appl. Mater. Interfaces*, 2014, **6**, 12214–12225.
27 Y. Zhao, H. M. Wong, W. Wang, P. Li, Z. Xu, E. Y. Chong, C. Yan, K. W. Yeung and P. K. Chu, *Biomaterials*, 2013, **34**, 9264–9277.
28 Z. Novotna, A. Reznickova, S. Rimpelova, M. Vesely, Z. Kolska and V. Svorcik, *RSC Adv.*, 2015, **5**, 41428–41436.
29 A. A. John, A. P. Subramanian, M. V. Vellayappan, A. Balaji, S. K. Jaganathan, H. Mohandas, T. Paramalinggam, E. Supriyanto and M. Yusof, *RSC Adv.*, 2015, **5**, 39232–39244.
30 R. K. Roeder, M. M. Sproul and C. H. Turner, *J. Biomed. Mater. Res.*, 2003, **67**, 801–812.

31 G. L. Converse, W. M. Yue and R. K. Roeder, *Biomaterials*, 2007, **28**, 927–935.
32 S. M. Tang, P. Cheang, M. S. Abu Bakar, K. A. Khor and K. Liao, *Int. J. Fatigue*, 2004, **26**, 49–57.
33 M. S. Abu Bakar, M. H. Cheng, S. M. Tang, S. C. Yu, K. Liao, C. T. Tan, K. A. Khor and P. Cheang, *Biomaterials*, 2003, **24**, 2245–2250.
34 J. Z. Liang, R. K. Y. Li and S. C. Tjong, *Polym. Compos.*, 1999, **20**, 413–422.
35 K. L. Fung, R. K. Y. Li and S. C. Tjong, *J. Appl. Polym. Sci.*, 2002, **85**, 169–176.
36 S. C. Tjong, S. L. Liu and R. K. Y. Li, *J. Mater. Sci.*, 1996, **31**, 479–484.
37 X. L. Xie, B. G. Li, Z. R. Pan, R. K. Y. Li and S. C. Tjong, *J. Appl. Polym. Sci.*, 2001, **80**, 2105–2112.
38 S. C. Tjong, *Carbon Nanotube Reinforced Composites: Metal and Ceramic Matrices*, Wiley-VCH, Winheim, Germany, 2009, pp. 1–228.
39 S. C. Tjong and Y. Z. Meng, *Polymer*, 1997, **38**, 4609–4615.
40 M. Colilla, B. González and M. Vallet-Regí, *Biomater. Sci.*, 2013, **1**, 114–134.
41 P. A. Tran, L. Sarin, R. H. Hurt and T. J. Webster, *J. Mater. Chem.*, 2009, **19**, 2653–2659.
42 V. B. Damodaran, D. Bhatnagar, V. Leszczak and K. C. Popa, *RSC Adv.*, 2015, **5**, 37149–37171.
43 Z. J. Han, A. E. Rider, M. Ishaq, S. Kumar, A. Kondyurin, M. M. Bilek, I. Levchenko and K. Ostrikov, *RSC Adv.*, 2013, **3**, 11058–11072.
44 K. Kavitha, W. Chunyan, D. Navaneethan, V. Rajendran, S. Valiyaveettil and A. Vinoth, *RSC Adv.*, 2013, **4**, 43951–43961.
45 J. Zhang and T. J. Webster, *Nano Today*, 2009, **4**, 66–80.
46 G. Suresh Kumar, L. Sathish, R. Govindan and E. K. Girija, *RSC Adv.*, 2014, **5**, 39544–39548.
47 H. Zhou and J. Lee, *Acta Biomater.*, 2011, **7**, 2769–2781.
48 S. K. Natarajan and S. Selvaraj, *RSC Adv.*, 2014, **4**, 14328–14334.
49 Z. Tao, *RSC Adv.*, 2014, **4**, 18961–18980.
50 M. Ghadiri, W. Chrzanowski and R. Rohanizadeh, *RSC Adv.*, 2015, **5**, 29467–29481.
51 M. Peran, A. A. Garcia, E. Lopez-Ruiz, G. Jimenez and J. A. Marchal, *Materials*, 2013, **6**, 1333–1359.
52 F. Mohandes and M. Salavati-Niasari, *RSC Adv.*, 2014, **4**, 25993–26001.
53 M. R. Rogel, H. Qiu and G. A. Ameer, *J. Mater. Chem.*, 2008, **18**, 4233–4241.
54 S. C. Tjong and S. P. Bao, *Compos. Sci. Technol.*, 2007, **67**, 314–323.
55 Y. C. Li, S. C. Tjong and R. K. Y. Li, *Synth. Met.*, 2010, **160**, 1912–1919.
56 S. C. Tjong and G. D. Liang, *Mater. Chem. Phys.*, 2006, **100**, 1–5.
57 L. He and S. C. Tjong, *RSC Adv.*, 2015, **5**, 15070–15076.
58 W. Bonfield, M. Wang and K. E. Tanner, *Acta Mater.*, 1998, **46**, 2509–2518.
59 K. Li, C. Y. Yuen, K. W. Yeung and S. C. Tjong, *Adv. Eng. Mater.*, 2012, **14**, B155–B165.
60 C. Z. Liao, H. M. Wong, K. W. K. Yeung and S. C. Tjong, *Mater. Sci. Eng., C*, 2013, **33**, 1380–1388.
61 J. Venkatesan and S. K. Kim, *J. Biomed. Nanotechnol.*, 2014, **10**, 3124–3140.
62 F. Sun, H. Zhou and J. Lee, *Acta Biomater.*, 2011, **7**, 3813–3829.
63 L. Wang, L. Weng, S. Song, Z. Zhang, S. Tian and R. Ma, *Mater. Sci. Eng., A*, 2011, **528**, 3689–3696.
64 C. Grabinski, S. Hussain, K. Lafdi, L. Braydich-Stolle and J. Schlager, *Carbon*, 2007, **45**, 2828–2835.
65 P. L. Price, M. Waid, K. Haberstroh and T. J. Webster, *Biomaterials*, 2003, **24**, 1877–1887.
66 J. Sandler, P. Werner, M. S. Shaffer, V. Demchuk, V. Altstad and A. H. Windle, *Composites, Part A*, 2002, **33**, 1033–1039.
67 T. Kokubo and H. Takadama, *Biomaterials*, 2006, **27**, 2907–2915.
68 A. J. Salinas and M. Vallet-Regi, *RSC Adv.*, 2013, **3**, 11116–11131.
69 W. D. Callister and D. G. Rethwisch, *Materials Science and Engineering: An Introduction*, John Wiley, New York, 9th edn, 2013.
70 G. Tetteh, A. S. Khan, R. M. Delaine-Smith, G. C. Reilly and I. U. Rehman, *J. Mech. Behav. Biomed. Mater.*, 2014, **39**, 95–110.
71 L. D. Silvio, M. J. Dalby and W. Bonfield, *Biomaterials*, 2002, **23**, 101–107.
72 R. N. Downes, S. Vardy, K. E. Tanner and W. Bonfield, *Bioceramics*, 1991, **4**, 239–246.
73 B. Gewert, M. M. Plassmann and M. MacLeod, *Environ. Sci.: Processes Impacts*, 2015, **17**, 1513–1521.
74 C. J. Hilado, *Flammability Handbook For Plastics*, Technomic Publishing Company Inc, Pennsylvania, USA, 5th edn, 1998, ch. 2.
75 L. H. Perng, C. J. Tsai and Y. C. Ling, *Polymer*, 1999, **40**, 7321–7329.
76 P. Patel, T. R. Hull, R. W. McCabe, D. Flath, J. Grasmeder and M. Percy, *Polym. Degrad. Stab.*, 2010, **95**, 709–718.
77 D. Bikiaris, A. Vassiliou, K. Chrissafis, K. M. Paraskevopoulos, A. Jannakoudakis and A. Docoslis, *Polym. Degrad. Stab.*, 2008, **93**, 952–967.
78 J. M. Worle-Knirsch, K. Pulskamp and H. F. Krug, *Nano Lett.*, 2006, **6**, 1261–1268.
79 J. Muller, H. Huaux and D. Lison, *Carbon*, 2006, **44**, 1048–1056.
80 A. Porter, M. Gass, K. Muller, J. N. Skepper, P. A. Midgley and M. Welland, *Nat. Nanotechnol.*, 2007, **2**, 713–717.
81 C. Z. Liao, H. M. Wong, K. W. K. Yeung and S. C. Tjong, *Int. J. Nanomed.*, 2014, **9**, 1299–1310.
82 A. K. Gaharwar, S. M. Mihaila, A. Swami, A. Patel, S. Sant and R. L. Reis, *Adv. Mater.*, 2013, **25**, 3329–3336.
83 G. S. Stein and J. B. Lian, *Endocr. Rev.*, 1993, **14**, 424–442.
84 E. K. Elias, P. L. Price and T. J. Webster, *Biomaterials*, 2002, **23**, 3279–3287.
85 X. Li, H. Gao, M. Uo, Y. Sato, T. Akasaka, Q. Feng, F. Cui, X. Liu and F. Watari, *J. Biomed. Mater. Res., Part A*, 2009, **91**, 132–139.
86 A. B. Zadpoor, *Mater. Sci. Eng., C*, 2014, **35**, 134–143.

87 J. Ni and M. Wang, *Mater. Sci. Eng., C*, 2002, **20**, 101–109.
88 W. Chrzanowski, W. J. Yeow, R. Rohanizadeha and F. Dehghani, *RSC Adv.*, 2012, **2**, 9214–9223.
89 T. Akasaka, F. Watari, Y. Sato and K. Tohji, *Mater. Sci. Eng., C*, 2006, **26**, 675–678.
90 H. M. Kim, T. Himeno, T. Kokubo and T. Nakamura, *Biomaterials*, 2005, **26**, 4366–4373.
91 N. M. Alves, I. B. Leonor, H. S. Azevedo, R. L. Reis and J. F. Mano, *J. Mater. Chem.*, 2010, **20**, 2911–2921.
92 F. Yang, S. K. Both, X. Yang, X. F. Walboomers and J. A. Jansen, *Acta Biomater.*, 2009, **5**, 3295–3304.
93 T. Liu, S. Wang, Z. Mo and H. Zhang, *J. Appl. Polym. Sci.*, 1999, **73**, 237–243.
94 J. N. Hay, J. I. Langford and J. R. Lloyd, *Polymer*, 1989, **30**, 489–493.